JOURNAL OF CATALYSIS 153, 333–343 (1995)

Amorphous Alloy Catalysis

VII. Activation and Surface Characterization of an Amorphous Cu–Ti Alloy Catalyst Precursor in the Dehydrogenation of 2-Propanol and Comparison with Cu–Zr[1]

Tamás Katona[2] and Árpád Molnár

Department of Organic Chemistry, Center for Catalysis, Surface and Material Science, József Attila University, Dóm tér 8, H-6720, Szeged, Hungary

Received March 14, 1994; revised January 30, 1995

The activation and catalytic properties of Cu–Ti and Cu–Zr metallic glass precursors in the dehydrogenation of 2-propanol differ substantially. In contrast with Cu–Zr, Cu–Ti can only be activated with HF solution. The pretreatment of Cu–Ti results in catalysts with BET and copper surface areas one order of magnitude smaller than those of Cu–Zr under the same conditions. Cu–Ti exhibits decreasing catalytic activity, while Cu–Zr displays stable activity in the course of the reaction. Crystallization of the metallic glasses prior to HF treatment results in a weaker reactivity toward hydrogen fluoride for both alloys. Scanning electron micrographs of the alloys reveal that HF etching results in surfaces with deep grooves, and copper-rich flakes, a Raney–Cu-like catalyst. Auger electron spectroscopic studies show copper enrichment in the surface region on both alloys after HF treatment. On the surface of Cu–Ti, mostly Cu(II) is detected, whereas Cu(0) and Cu(II) coexist on Cu–Zr. © 1995 Academic Press, Inc.

INTRODUCTION

The development of the melt quenching method (1, 2) led to amorphous alloys (metallic glasses) becoming available from the beginning of the 1980s and a large number of studies have been reported on their unique chemical and physical properties. Since polycrystalline bimetallic catalysts are widely used (3–5), and there is a strong structure dependence of the reaction rate in many reactions, the use of amorphous alloys in catalytic syntheses has likewise received considerable attention. The results show that these alloys exhibit outstanding catalytic properties in many cases. Review papers have been published on this topic (6, 7).

Cu–Zr metallic glasses have been tested as catalysts in reactions such as the hydrogenation of CO (8–10), CO_2 (10, 11), ethylene (12, 13) and 1,3-butadiene (14). Amorphous Cu–Zr catalyst precursors and Cu–Ti alloys have been tested and compared only in the decomposition of methanol (15, 16). We earlier studied the dehydrogenation of 2-propanol over $Cu_{61}Zr_{39}$ alloys (17–22). In all of these experiments, following various kinds of activation, the amorphous alloys exhibit higher catalytic activity than the crystalline catalysts used for comparison. During the activation and reaction, the amorphous precursors underwent substantial structural changes, resulting in crystalline catalysts with higher activity than that of the originally crystalline alloy with the same composition.

Cu–Zr metallic glasses have been found to be excellent catalyst precursors for the dehydrogenation of 2-propanol. This corresponds to the literature finding that copper, among other metals (23), catalyzes the dehydrogenation of alcohols (24–27) and diols (28–34), the dehydration of diols (35–37), and the hydrogenolysis of the C–O bond (38–42). However, no data are available on Cu–Ti alloys, one of the most obvious choices for comparison, except for our earlier observation (22) that Cu–Ti in the as-received and oxidized state dehydrates 2-propanol at 673 K. The purpose of the present study was to obtain data on a Cu–Ti amorphous alloy in the same test reaction used previously to characterize Cu–Zr metallic glasses under identical conditions. Surprisingly, the activation methods (H_2/473 K (10, 11), H_2/573 K (17–19), H_2O/500 K (8, 9) HF/5 min (15, 16)) that resulted in high catalytic activity for Cu–Zr catalysts (17, 18) were not effective for Cu–Ti alloys, with the exception of HF treatment (21). In the present paper we report on the use of a Cu–Ti amorphous alloy activated with HF solution as catalysts, in the dehydrogenation of 2-propanol. We focus on the effects of HF on the catalytic activity, structure, and surface of Cu–Ti alloys. Their catalytic performance will be compared with that of Cu–Zr metallic glasses by referring to the results of previous catalytic tests (17). New results on the mor-

[1] Part VI: see Ref. (22).

[2] To whom correspondence should be addressed.

0021-9517/95 $6.00

TABLE 1

Results of Surface Area Measurements of the Amorphous and Crystalline Cu–Ti and Cu–Zr Alloys after HF Treatment and after Reaction

Catalyst	Structure	Time of HF treatment (min)	BET surface area ($m^2 g^{-1}$)		Cu(0) surface area ($m^2 g^{-1}$)	
			After HF treatment	After activation and reaction (24 h)	After HF treatment	After activation and reaction (24 h)[a]
Cu–Ti	Amorphous	—			0.01[b]	—[c]
		1			0.01[b]	—[c]
		3			–	—[c]
		5	0.1	0.6	0.03	0.03 (0.03)[d]
	Crystalline	—			—[c]	—[c]
		5			0.01[b]	0.01[b]
Cu–Zr	Amorphous	—			0.01[b]	0.19
		1			0.14	0.24
		3			0.40	0.96
		5	4.1	4.6	0.41	1.03 (1.00)[d]
	Crystalline	—			0.01[b]	0.45
		5			0.06	0.28

[a] After exposed to air catalyst samples were activated at 573 K in flowing hydrogen (30 ml min^{-1}) for 0.5 h before measurement.
[b] Detection limit.
[c] Not measurable, being under the detection limit.
[d] Surface area determined *in situ* after reaction.

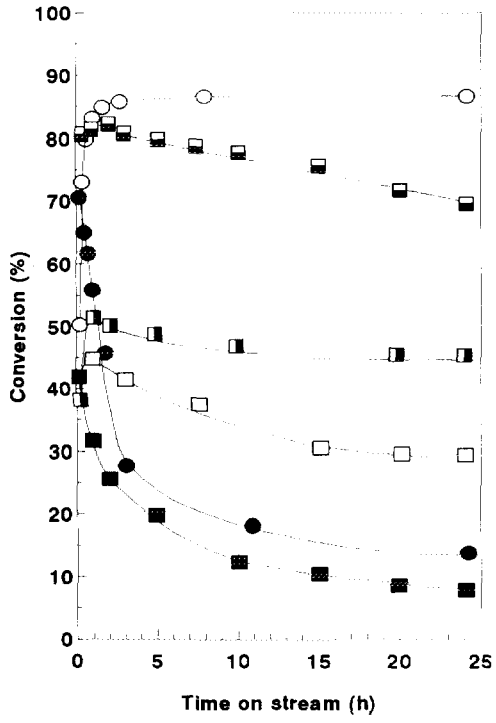

FIG. 1. Conversion of 2-propanol over amorphous and crystalline HF-treated Cu–Ti and Cu–Zr alloys as a function of time on stream (T = 573 K). (○) Amorphous Cu–Zr treated with HF/5 min; (●) crystalline Cu–Zr treated with HF/5 min; (◧) amorphous Cu–Ti treated with HF/1 min; (◒) amorphous Cu–Ti treated with HF/3 min; (□) amorphous Cu–Ti treated with HF/5 min; (■) crystalline Cu–Ti treated with HF/3 min.

phology, surface structure, and depth profile of HF-treated Cu–Zr alloys will also be discussed.

EXPERIMENTAL

Two-millimeter-wide, 100-μm-thick $Cu_{61}Zr_{39}$ and $Cu_{50}Ti_{50}$ ribbons were produced by the melt quenching method in air at a cooling wheel velocity of 2000 cm s^{-1}.

The catalytic tests were carried out in a flow-type microreactor (573 K, about 50 mg alloy, 30 ml min^{-1} hydrogen carrier gas). The vapor of 2-propanol was introduced through a saturator. An ice-cooled trap was inserted between the reactor and the saturator to obtain reproducible reactant flow. The reaction products were subjected to GC analysis. A detailed description of the experimental setup is given in (17). Kinetic studies were performed using a small catalyst quantity and a high feeding rate to ensure low conversion (below 10%).

TABLE 2

Catalytic Activity of HF-treated Cu–Ti and Cu–Zr Alloys in the Dehydrogenation of 2-Propanol (HF Treatment, 5 Min)

Catalyst	Rate based on catalyst mass (mol $g^{-1} s^{-1}$)	Rate based on BET surface (mol $m^{-2} s^{-1}$)	Rate based on Cu(0) surface (s^{-1})
Cu–Ti	1.10×10^{-4}	1.83×10^{-4}	156
Cu–Zr	3.24×10^{-4}	0.70×10^{-4}	14

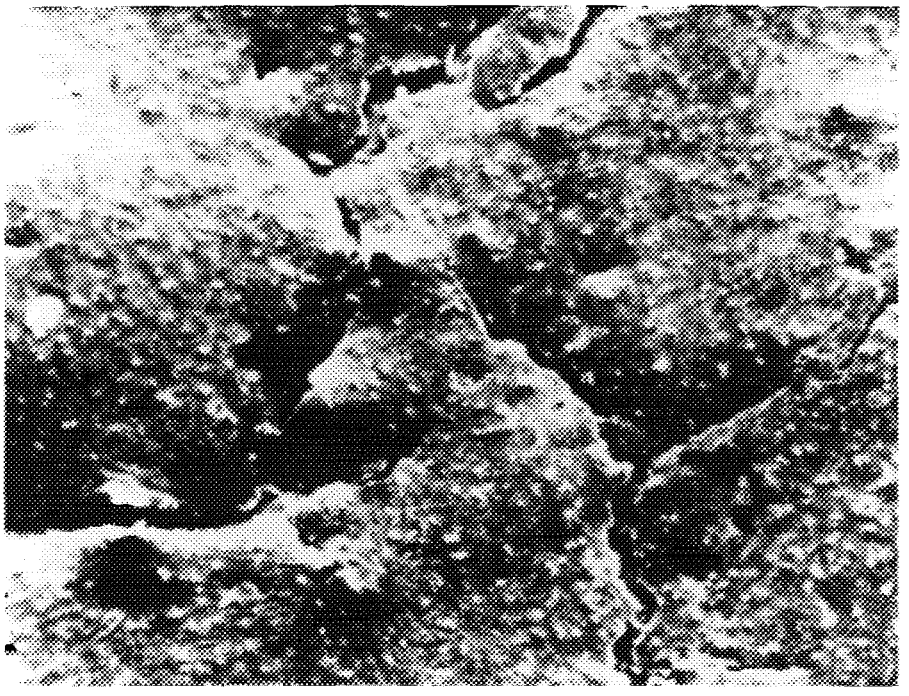

FIG. 2. Scanning electron micrograph of a Cu–Zr sample after 5 min HF treatment. Both sides of the ribbon feature the same morphology (1000×).

The amorphous alloys were activated with 1 *M* HF solution, washed with H_2O, and put into the reactor while still wet. They were allowed to dry at room temperature in the carrier gas stream. The crystalline alloys were made by annealing the metallic glass samples under helium at 773 K for 10 min. The complete crystallization of the originally amorphous alloys was proved by differential scanning calorimetry (DSC) and X-ray diffraction (XRD).

BET surface areas were determined using nitrogen adsorption at 77 K. The Cu(0) surface area of the catalysts was measured by N_2O titration based on the reaction of nitrous oxide with Cu(0) species. The GC pulse method (43), with the modifications suggested in (44), was used (363 K, small sample size, large excess of N_2O). When the catalyst samples after reaction were exposed to air, a reactivation in flowing hydrogen (573 K, 0.5 h, 30 ml min^{-1}) was applied before surface measurements.

The structure of the alloys was tested by DSC (Perkin–Elmer DSC 2) and XRD (DRON 3 apparatus, Cu$K\alpha$ radiation). The surface of the alloys was investigated by scanning electron microscopy (SEM) with an ISI DS 130 instrument, scanning Auger microscopy (SAM) with a Perkin–Elmer PHI 660 unit, and X-ray photoelectron spectroscopy (XPS) with a Perkin–Elmer PHI 5300 apparatus with 1253.6 eV Mg$K\alpha$ radiation. A stainless-steel sample holder with Mo mounting plates was used. The Mo $3d_{5/2}$ signals were used for calibration. For depth profile measurements, a 3 kV Ar ion beam rastered over a 10 × 10 mm area and a 5 kV unrastered Ar ion beam were used for XPS and SAM experiments, respectively.

RESULTS

Over both alloys, the dehydrogenation of 2-propanol occurred selectively to acetone at 573 K. The formation of 4-methyl-2-pentanone, a condensation product of acetone, was detected only over Cu–Zr catalysts prepared from amorphous precursors. The selectivity of this by-product was always less than 5%. Over Cu–Ti, in turn, a small amount of propene was formed.

Figure 1 summarizes the changes in activity of the amorphous and crystalline Cu–Zr and Cu–Ti precursors after different HF pretreatments. Amorphous Cu–Zr exhibits an induction period, followed by stable and high catalytic activity. The previously crystallized Cu–Zr alloy displays substantially lower activity which decreases in the course of the reaction. The catalytic performances of Cu–Ti alloys are weaker than those of the corresponding Cu–Zr alloys. The activity vs time-on-stream curves exhibit maxima during the first 5 h of the run. The previously crystallized alloys give similar curves with a lower activity than that of the crystalline Cu–Zr alloys. The as-received Cu–Ti alloys do not show catalytic activity. This is in contrast to the as-received Cu–Zr alloys, which exhibit continuously increasing catalytic activity during the reaction (17).

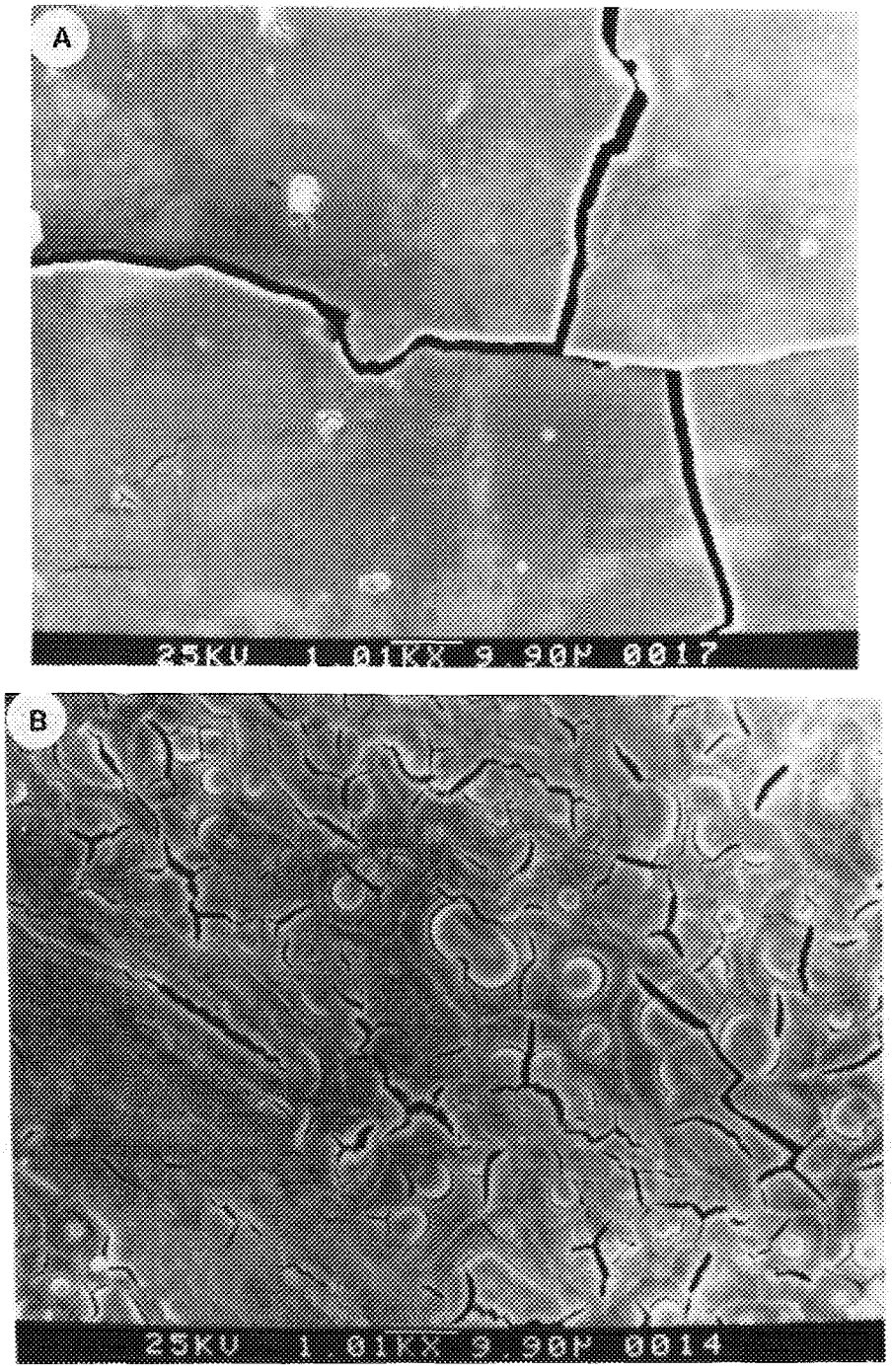

FIG. 3. Scanning electron micrograph of an amorphous Cu–Ti sample after 3 min HF treatment. The horizontal bar above the magnification value corresponds to the distance specified in μm; (A) outer side 1010×; (B) inner side 1010×; and (C) outer side 40,300×.

The results of BET and Cu(0) surface area measurements are summarized in Table 1. The as-received alloys have a very small surface area in the range of the geometrical surface. After HF treatment, the amorphous Cu–Zr exhibits large BET and Cu(0) surfaces, which are further increased as a result of the reaction. The Cu–Ti alloys, in contrast, exhibit an increase in surface areas one order of magnitude smaller than that of Cu–Zr during the identical treatment. Crystallization does not bring about any enhancement of the Cu(0) surface area. A relatively small increase, as compared with that for the amorphous alloy, can be monitored on crystalline Cu–Zr after HF treatment. A further increase takes place during the reaction. No similar changes are observed on Cu–Ti.

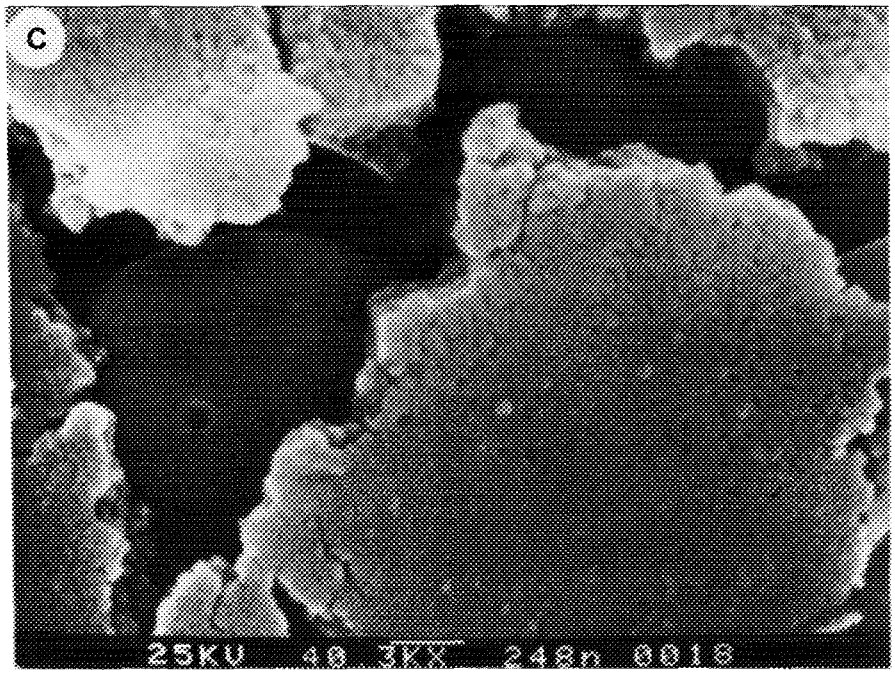

FIG. 3—*Continued*

Specific catalytic activities calculated using activities determined at low conversion (below 10%) and the appropriate surface area values are summarized in Table 2.

In accordance with XRD measurements, DSC experiments revealed the total crystallization of Cu–Zr alloys as a result of HF treatment (17). Only partial crystallization is found in Cu–Ti alloys after HF treatment. This state is conserved during the reaction, i.e., no further crystallization can be detected as a result of the catalytic reaction.

The surfaces of the two sides of the as-received alloys show the characteristics of metallic glasses prepared by melt quenching methods (12, 18, 19) with the single wheel technique. The inner sides feature small, parallel grooves due to the contact with the cooling wheel. The outer sides exhibit large randomly located hillocks. In the 0.1–1-μm size range; however, no characteristic features can be found. Since Zr/ZrO_x and Ti/TiO_x dissolve in HF more readily than Cu, HF treatment results in drastic changes in surface morphology. On both sides of the Cu–Zr ribbons, large flakes develop (Fig. 2). On Cu–Ti, round grooves appear on the outer side, while the inner side resembles the HF-treated Cu–Zr alloys (Fig. 3).

The surface morphology of HF-treated Cu–Ti alloys was investigated by means of scanning Auger microscopy combined with Ar ion sputtering. This was done by using an unrastered 5 keV Ar ion beam resulting in a high sputtering rate. Scanning along the cross section of the crater thus created allows study of the changes both in morphology and composition at various depths. Figure 4 shows scanning electron micrographs of the sputtered area at various magnifications and locations. Figure 5 presents the corresponding Auger spectra. In Fig. 4A, a bright and a dark area are separated along a boundary line. This is the region where HF penetrated the ribbon. Figure 4B shows the boundary region at higher magnification. Flake formation occurs as a result of HF etching. In the darker areas, no flakes can be seen, but the round grooves can still be traced (Fig. 4C). These are surrounded by hillocks and cones of almost pure copper (Fig. 5, spectrum D). Next to these, the smooth area contains both Cu and Ti with the composition of the original amorphous alloy (Fig. 5, spectrum E).

The results of the XPS experiments are to be seen in Figs. 6–9. The XPS multiplex spectra in the C 1*s*, Cu $2p_{3/2}$, Ti $2p_{3/2}$ (or Zr $3d_{5/2}$) and O 1*s* binding energy ranges are plotted after each minute of Ar-sputtering, along with the depth profiles, by using the integrated peak intensities of these elements. Bombardment was carried out by using a 3-kV Ar ion beam. Because of the poor spatial resolution of the X-ray beam, the Ar ion beam was rastered to obtain uniform depth. This resulted in a considerably lower sputtering rate than in the case of the SAM experiments, i.e., the data obtained relate to the near surface region of the alloys. The multiplex spectra of each region are adjusted to fit the scale, i.e., they are drawn in arbitrary units.

Copper concentration in the as-received Cu–Ti alloys is negligible on both sides (Fig. 6). On the outer side, it increases continuously in the depth range investigated. On the inner side, there is a relative copper enrichment as compared with the outer side. On the outer side, the

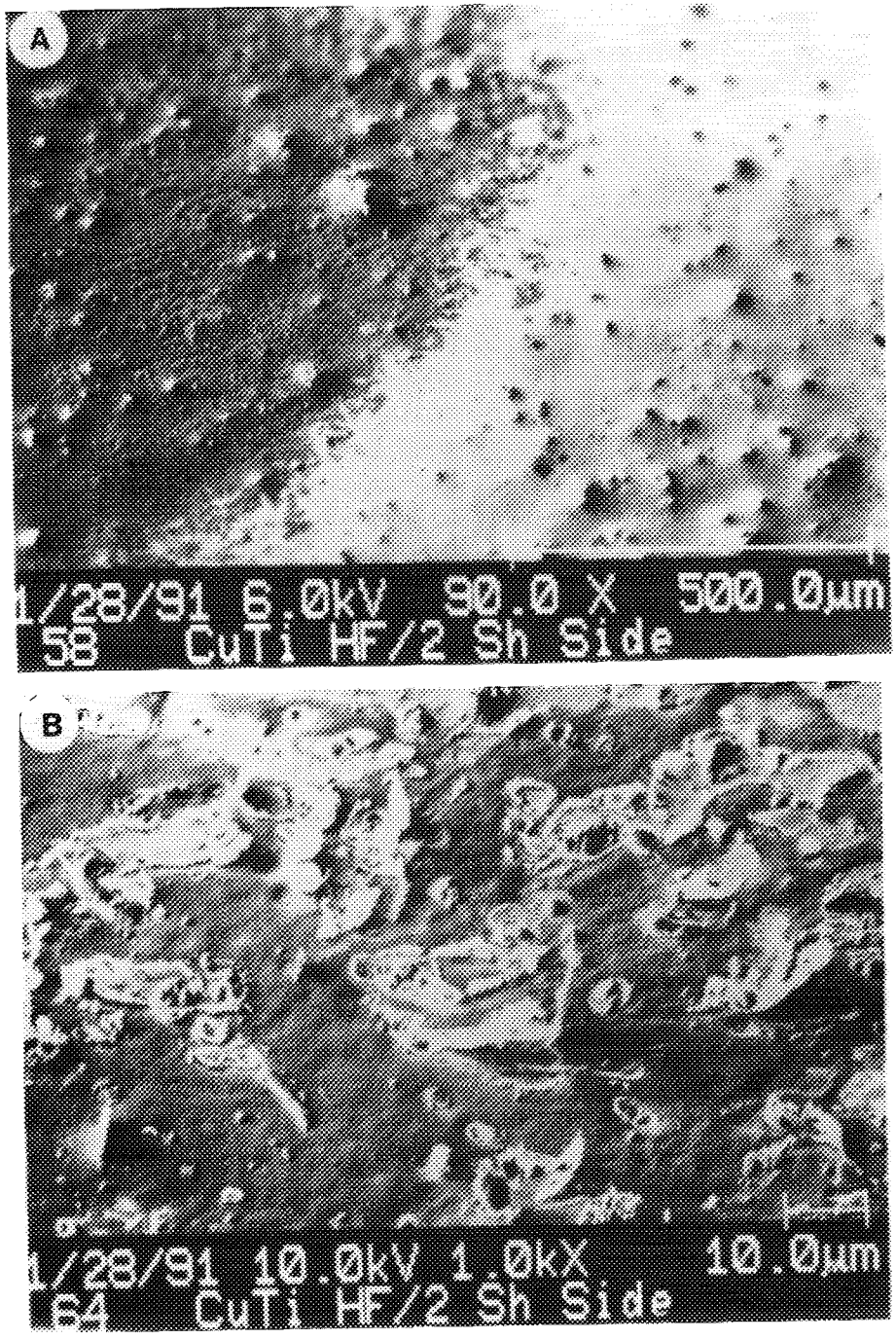

FIG. 4. Scanning electron microscopic pictures of the outer side of an HF-treated Cu–Ti sample after 10 min Ar ion sputtering in the SAM instrument. The scale bar is indicated on the bottom right of the pictures; (A) boundary region where HF penetrated the ribbon (90×); (B) flake formation in the boundary region (1000×); (C) round grooves in the sputtered area (5000×).

intensity of the oxygen peak decreases continuously in parallel with the continuously increasing intensity of the Ti $2p_{3/2}$ peak at 454 eV, characteristic of metallic Ti. Although a considerable amount of Ti is oxidized on the surface, the convoluted spectrum shows the presence of metallic Ti as well. This effect is more significant on the inner side, where mostly TiO_2 (457 eV) is found on the surface. After 10 min of sputtering the composition changes sharply to mostly metallic Ti (454 eV) at the same depth as where the intensity of the oxygen peak drops.

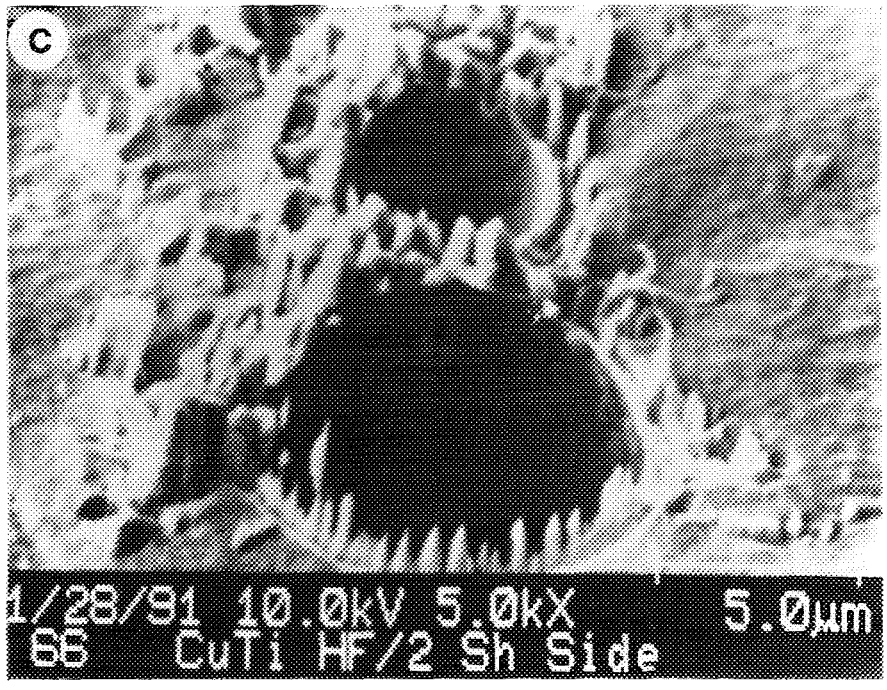

FIG. 4—*Continued*

There is no visible shift in the copper spectra; they are characteristic of metallic Cu throughout the depth investigated.

The XPS depth profiles of the two sides of an HF-treated Cu–Ti alloy are shown in Fig. 7. There is copper enrichment on both sides. The concentration of titanium decreases substantially as a result of HF treatment with a peak only in the range of the background noise. The alloy still contains some oxygen. We believe that this is bound to Ti, because the copper signals show mainly the presence of Cu(0) species in the bulk.

The XPS depth profiles of the two sides of the Cu–Zr alloys after HF treatment are shown in Fig. 8. Similarly as for the Cu–Ti alloys, copper enrichment is seen on both sides, but its concentration does not increase continuously toward the bulk. On the outer side, the Zr and O

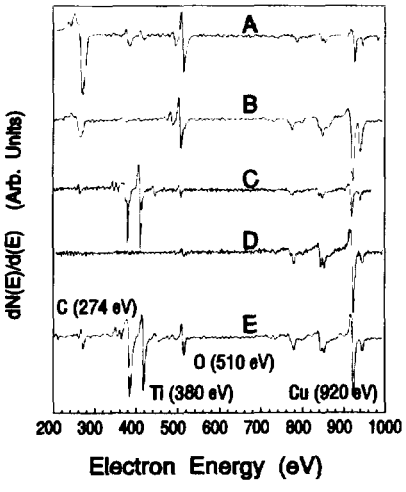

FIG. 5. Auger spectra of the different surface species of HF-treated sputtered Cu–Ti alloy shown in Fig. 4; (A) unsputtered area; (B) area after 1 min sputtering; (C) AES spectrum of a flake; (D) cone structure in the sputtered area; and (E) smooth area next to the cone structure.

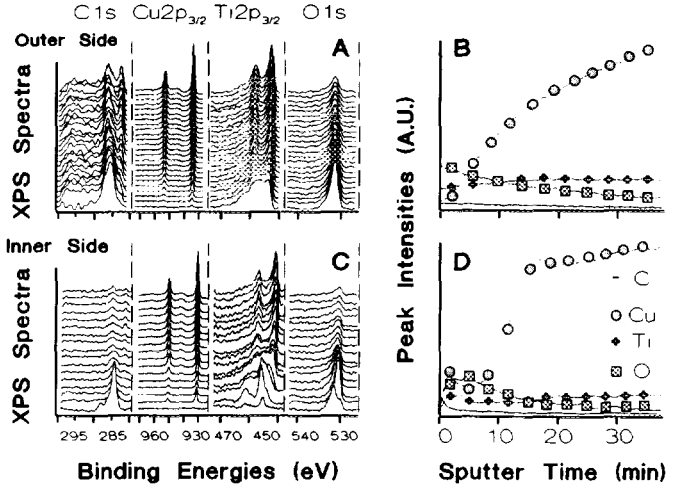

FIG. 6. XPS multiplex spectra and depth profiles based on the intensities of each component of the two sides of the as-received Cu–Ti alloys. (A and C) multiplex spectra; (B and D) depth profiles; (A and B) outer side, (C and D) inner side; (—) carbon; ( ) copper; ( ) titanium; ( ) oxygen.

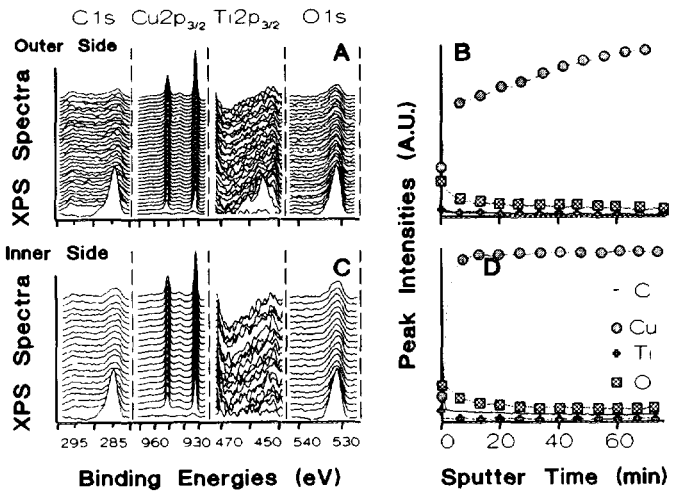

FIG. 7. XPS multiplex spectra and depth profiles based on the intensities of each component of the two sides of the HF-treated Cu–Ti alloy. (A and C) multiplex spectra; (B and D) depth profiles; (—) carbon; ( ) copper; ( ) titanium; ( ) oxygen.

signals change in parallel until the concentration of oxygen drops sharply. In this region, the Zr binding energy shifts from that of the oxidized state (182 eV) to that of the reduced state (179 eV). On the inner side, however, the intensities of the Zr and O peaks change in parallel and the Zr remains in the oxidized state throughout the depth of the investigation.

In Fig. 9, the copper multiplex spectra of HF-treated Cu–Ti and Cu–Zr alloys are compared on the surface without sputtering and in the bulk after 30 minutes of Ar ion sputtering. On the surface, Cu–Ti exhibits only Cu(II) species with the characteristic $2p_{3/2}$ peak at 933.6 eV, the

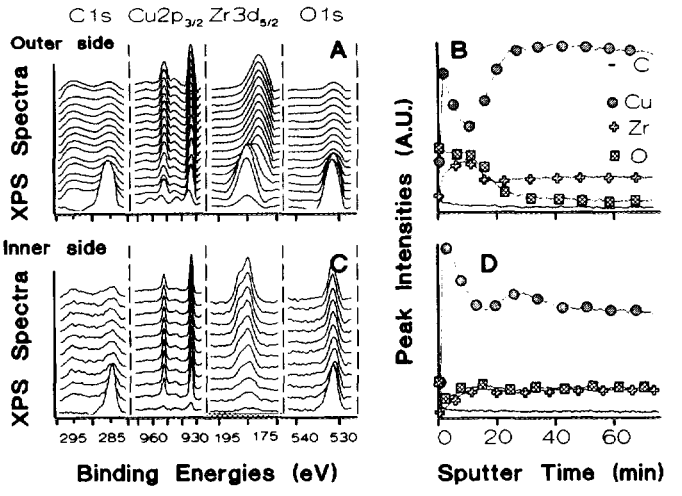

FIG. 8. XPS multiplex spectra and depth profiles based on the intensities of each component of the two sides of the HF-treated Cu–Zr alloy. (A and C) multiple spectra; (B and D) depth profiles; (—) carbon; ( ) copper; ( ) zirconium; ( ) oxygen.

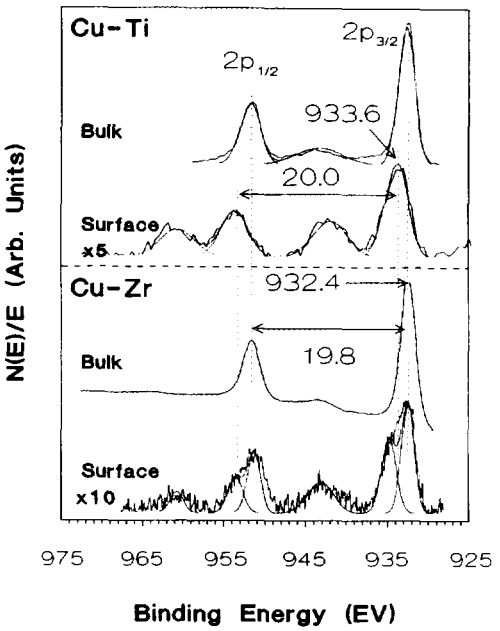

FIG. 9. Comparison of the Cu XPS multiplex spectra in the bulk and on the surface of Cu–Ti and Cu–Zr alloys.

$2p_{1/2}$ peak at 953.6 eV, and the "shake-up" peaks due to the paramagnetic feature of Cu(II). On the surface of the Cu–Zr alloy, however, Cu(II) and Cu(0) species coexist. The deconvolution of the multiplex spectrum shows the presence of Cu(0) with the characteristic $2p_{3/2}$ and $2p_{1/2}$ binding energies at 932.4 and 952.2 eV, respectively.

DISCUSSION

The comparison of the catalytic performance of Cu–Ti and Cu–Zr alloys in the dehydrogenation of 2-propanol after HF pretreatment shows some differences in activities (conversion) and stabilities (Fig. 1).

One of the substantial differences between the two amorphous alloys is the very difficult activation of Cu–Ti. The as-received amorphous Cu–Ti alloys did not show catalytic activity in the dehydrogenation of 2-propanol at 573 K. Hydrogen treatment and activation with H_2O vapor, which resulted in high activity for Cu–Zr metallic glasses (17), were not successful in the case of Cu–Ti (20). All such methods of activation caused devitrification of the amorphous state of Cu–Zr, as judged by either DSC or XRD (17–19). However, the crystalline phase formed during the reaction exhibited higher catalytic activity (if compared on the basis of catalyst mass) than that of the crystalline alloys prepared by annealing in an inert atmosphere.

Literature evidence exists showing that the amorphous Cu–Zr catalyst precursors undergo substantial structural changes during catalytic reactions resulting in the com-

plete crystallization of their bulk (12, 17). The active form of the catalyst develops in the course of the reaction. The originally crystalline alloys exhibit considerably lower catalytic activity. This can be explained if it is assumed that the amorphous state is more reactive to form a mixture of polycrystalline phases with better catalytic performance. This is supported by our comparative findings on Cu–Ti and Cu–Zr alloys.

During activation with hydrogen or water vapor, a considerable amount of copper segregates onto the surface of Cu–Zr alloys (9, 12, 17). We did not observe such copper segregation in Cu–Ti alloys, showing that they are not reactive from this point of view. Similarly, these methods of activation did not result in crystallization in Cu–Ti alloys, as judged by DSC and XRD. It is also seen that the amorphous state itself is not active, and an appropriate means of activation is needed to obtain catalytic activity.

Only HF treatment, the most drastic method, appears to be a successful means of activating Cu–Ti alloys. Even with this, the weight loss of Cu–Ti is about one-third that of Cu–Zr, leading to the exposure of significantly less copper. As a result of this activation, only partial crystallization occurred as compared with the complete crystallization of Cu–Zr after identical treatment. The reactivity of the crystallized alloys toward HF is strongly inhibited; the time necessary to attain the same weight loss by dissolving TiO_x (ZrO_x) is tripled when crystalline ribbons are treated.

The increase in catalytic activity of Cu–Zr samples in time on stream can be attributed to the further increase in copper surface. This is effected by hydrogen formed during the reaction and evidenced by the higher Cu(0) values measured after reaction (Table 1). Changes in the relative amount of Cu(0) and Cu(II) species (*vide infra*) may also affect catalytic activity which might be the reason for the decreasing activity of the Cu–Ti alloy. Another possibility (suggested by one of the referees) can be an SMSI effect (45, 46), although the temperature used in the present study is apparently rather low compared with that observed for Cu on TiO_2 catalysts (47, 48). However, the small amount of water formed as a result of dehydration of 2-propanol can result in the formation of TiO_2 from the amorphous phase still present. This *in situ*-formed TiO_2 may be capable of wetting copper, contributing to decreasing activities.

Since comparative studies have not been carried out, one can only speculate about the reasons for the striking difference in the activation of the two alloys. It is known that Cu–Zr undergoes structural changes even at room temperature. Our own experience shows that copper segregation on the inner side of the ribbon takes place within a few weeks after fabrication, manifested by the appearance of the characteristic red color of copper. Auger electron spectroscopy, accordingly, indicates copper enrichment (19). Incipient crystallization and bulk amorphous structure are detected by XRD and DSC, respectively. No similar transformation of Cu–Ti is observed. The difference in electronic interactions due to different electronegativities of the two metals and the difference in size of Ti and Zr may bring about chemical and structural heterogeneities in Cu–Zr, facilitating easy activation. In addition, oxygen present in our alloy samples due to fabrication conditions (melt quenching in air) may also contribute to the difference in behavior of the two alloys. Particularly, *in situ* formation of TiO_2 and wetting of copper (SMSI effect) during attempted activations and reactions may explain the difficulties in transforming Cu–Ti into an active catalyst. In contrast, the structural changes already taken place can induce the easy transformation of the Cu–Zr precursor under various activation conditions to generate active and stable supported copper catalysts.

The results of surface area measurements show substantial differences between the two alloys resulting from the different sensitivity to activation. Surface areas measured on Cu–Ti alloys by the BET method and using N_2O titration are one order of magnitude smaller as compared with Cu–Zr (Table 1). Rate data based on catalyst mass and BET surfaces are quite similar (Table 2). Rates calculated with Cu(0) data, in turn, seem to be unreasonably high for a heterogeneous catalytic reaction. This suggests that metallic copper surface, in this case, may not be an appropriate measure to represent the catalytically active sites in the dehydrogenation of 2-propanol. Indeed, it was already observed that both metallic and ionic copper play roles in the reaction (49–51), although the role of different oxidation states of copper is debated (52).

The XPS depth profile measurements suggest that in the bulk of the Cu–Zr and Cu–Ti alloy copper exists mostly in the metallic form. The oxygen is bound to Zr or Ti due to their higher affinity toward O. This is supported by the parallel changes in the intensity and peak shapes. In the bulk, oxygen exists mostly in the form of ZrO_x or TiO_x, but their contributions to the XPS signal are small as compared with the reduced form of Zr or Ti; thus they are concealed in the slope or in the background. The scanning Auger spectrum of the bulk (Fig. 5, spectrum E) demonstrates the presence of both oxygen and carbon besides the main components of the alloys, while HF treatment (which removes Ti preferentially) results in removal of the oxygen peak, also (Fig. 5, spectrum D). It should be mentioned that the carbon spectra on the outer side of the as-received Cu–Ti alloy exhibit a peak at 282 eV which is characteristic of the carbides. This can originate from the method of alloy fabrication, since the precursor alloys were melted in air and spun onto the cooling wheel without use of a protective atmosphere. This carbide peak is completely removed when HF treatment is applied (Fig. 7).

On the surface of Cu–Zr both metallic and ionic copper can be found. It should be mentioned that it is rather difficult to make a difference between Cu(0) and Cu(I), since the difference between their $2p_{3/2}$ binding energies is less than 0.5 eV. To distinguish the two species, investigation of the $CuL_3M_{45}M_{45}$ Auger transition is used (49–51), as well as the calculation of the Auger parameter (α) (53, 54). In our case, in agreement with the results of Cunningham *et al.* (49–51), the $CuL_3M_{45}M_{45}$ kinetic energy is found at around 920 eV which suggests that copper is in the metallic state in the bulk. Therefore no evidence is found for the presence of Cu(I).

SUMMARY

A comparison of Cu–Ti and Cu–Zr metallic glasses reveals both similarities and differences, which can be explained by taking into account the initial amorphous states, which affect their chemical behavior. The amorphous state, in general, is more reactive toward HF and, as a result of a dynamic interaction, the active form of the catalyst emerges. This reactivity ceases when the alloys are crystallized by annealing in an inert atmosphere, i.e., crystallization strongly inhibits their solubility in HF.

In the case of Cu–Ti, AES experiments indicate that only the chemical removal of Ti/TiO_x with HF results in a copper-rich surface. However, on this surface, a very small amount of Cu(0) is detected by means of nitrous oxide titration whereas XPS measurement indicates mostly Cu(II) species. In contrast, Cu–Zr catalysts possess the two species on their surfaces in comparable amounts. No direct correlation is found between catalytic activity and Cu(0) surface area determined by nitrous oxide titration in alcohol dehydrogenation.

ACKNOWLEDGMENTS

The authors thank Z. Hegedüs and Cs. Kopasz for the amorphous alloy samples, and acknowledge the support provided for this research by the Hungarian National Science Foundation through Grants OTKA 1885 and T4311.

REFERENCES

1. Duwez, P., *Trans. Am. Soc. Met.* **60,** 607 (1967).
2. Pond, R., Jr., and Salli, I. V. *TMS-AIME* **245,** 2475 (1969).
3. Sinfelt, J. H., and Cusumano, J. A., *in* "Advanced Materials in Catalysis," (J. J. Burton, and R. L. Garten, Eds.), p. 1. Academic Press, New York, 1977.
4. Sachtler, W. M. H., and van Santen, R. A., *Adv. Catal.* **26,** 69 (1977).
5. Ponec, V., *Adv. Catal.* **32,** 149 (1983).
6. Molnár, A., Smith, G. V., and Bartók, M., *Adv. Catal.* **36,** 329 (1989).
7. Baiker, A., *in* "Metallic Glasses III" (H. Beck, and H.-J. Güntherodt, Eds.), p. 121. Springer, Berlin, 1993; *Faraday Discuss. Chem. Soc.* **87,** 239 (1989).
8. Shibata, M., Ohbayashi, Y., Kawata, N., Masumoto, T., and Aoki, K., *J. Catal.* **96,** 296 (1985).
9. Shibata, M., Kawata, N., Masumoto, T., and Kimura, H. M., *J. Catal.* **108,** 263 (1987).
10. Schild, C., Woukan, A., and Baiker, A., *J. Mol. Catal.* **63,** 243 (1990).
11. Gasser, D., and Baiker, A., *Appl. Catal.* **48,** 279 (1989).
12. Baiker, A., Baris, H., and Guntherodt, H. J., *Appl. Catal.* **22,** 389 (1986).
13. Yamashita, H., Yoshikawa, M., Kaminade, T., Funabiki, T., and Yoshida, S., *J. Chem. Soc. Faraday Trans. 1* **82,** 707 (1986).
14. Baiker, A., Baris, H., and Guntherodt, H. J., *J. Chem. Soc. Chem. Commun.*, 930 (1986).
15. Yamashita, H., Kaminade, T., Yoshikawa, M., Funabiki, T., and Yoshida, S., *C, Mol. Chem.* **1,** 491 (1986).
16. Yoshida, S., Kakehi, T., Matsumoto, S., Tanaka, T., Kanai, H., and Funabiki, T., *in* "Proceedings, 10th International Congress on Catalysis, Budapest, 1992" (L. Guczi, F. Solymosi, and P. Tétényi, Eds.), *New Frontiers in Catalysis*, p. 981. Akadémiai Kiadó, Budapest, 1993.
17. Molnár, Á., Katona, T., Bartók, M., and Varga, K., *J. Mol. Catal.* **64,** 41 (1991).
18. Katona, T., Hegedüs, Z., Kopasz, Cs., Molnár, Á., and Bartók, M., *Catal. Lett.* **5,** 351 (1990).
19. Molnár, Á., Katona, T., Bartók, M., Perczel, I. V., Hegedüs, Z., and Kopasz, Cs., *Mater. Sci. Eng. A* **134,** 1083 (1991).
20. Katona, T., Molnár, Á., Perczel, I. V., Kopasz, Cs., and Hegedüs, Z., *Surf. Interface Anal.* **19,** 519 (1992).
21. Molnár, Á., Katona, T., Kopasz, Cs., and Hegedüs, Z., *in* "Proceedings, 10th International Congress on Catalysis, Budapest, 1992" (L. Guczi, F. Solymosi, and P. Tétényi, Eds.), *New Frontiers in Catalysis*, p. 1759. Akadémiai Kiadó, Budapest, 1993.
22. Katona, T., Molnár, Á., and Bartók, M., *Mater. Sci. Eng. A* **181/182,** 1095 (1994).
23. Bartók, M., Czombos, J., Felföldi, K., Gera, L., Göndös, Gy., Molnár, Á., Notheisz, F., Pálinkó, I., Wittmann, Gy., and Zsigmond, Á. G., "Stereochemistry of Heterogeneous Metal Catalysis." Wiley, Chichester, 1985.
24. Patterson, W. R., Roth, J. A., and Burwell, J. R., Jr., *J. Am. Chem. Soc.* **93,** 839 (1971).
25. Bartók, M., Notheisz, F., and Török, I., *Acta Phys. Chem.* **17,** 101 (1971).
26. Bartók, M., *Acta Phys. Chem. Szeged* **20,** 443 (1974).
27. Bartók, M., and Török, I., *Acta Chim. Acad. Sci. Hung.* **88,** 35 (1976).
28. Bartók, M., and Kozma, B., *Acta Phys. Chem. Szeged* **9,** 116 (1963).
29. Bartók, M., and Zalotai, L., *Acta Phys. Chem. Szeged* **14,** 39 (1968).
30. Zalotai, L., and Bartók, M., *Acta Phys. Chem. Szeged* **14,** 47 (1968).
31. Bartók, M., and Prágai, B., *Acta Phys. Chem. Szeged* **18,** 85 (1972).
32. Molnár, Á., and Bartók, M., *Acta Chim. Acad. Sci. Hung.* **89,** 393 (1976).
33. Molnár, Á., and Bartók, M., *J. Catal.* **72,** 322 (1981).
34. Bartók, M., *Magy. Kem. Lapja* **37,** 193 (1982).
35. Shuikin, N. I., Bartók, M., Karakhanov, R. A., and Shostakovsky, V. M., *Acta Phys. Chem. Szeged* **9,** 124 (1963).
36. Bartók, M., and Molnár, Á., *Acta Chim. Acad. Sci. Hung.* **100,** 203 (1979).
37. Bartók, M.; Molnár, Á. *in* "The Chemistry of Ethers, Crown Ethers, Hydroxyl Groups and their Sulphur Analogues" Supplement E (S. Patai, Ed.), p. 721. Wiley, New York, 1980.
38. Shuikin, N. I., Kovács, Ö., Bel'sky, I. F., and Bartók, M., *Dokl. Akad. Nauk SSSR* **136,** 1120 (1961).
39. Bartók, M., and Karakhanov, R. A., *Acta Phys. Chem. Szeged* **20,** 453 (1974).

40. Bartók, M., and Molnár, Á., *J. Chem. Soc. Chem. Commun.*, 1089 (1982).
41. Notheisz, F., Bartók, M., and Zsigmond, Á. G., *React. Kinet. Catal. Lett.* **29,** 339 (1985).
42. Notheisz, F., Molnár, Á., Zsigmond, Á. G., and Bartók, M., *J. Catal.* **98,** 131 (1986); *Magy. Kem. Foly.* **94,** 24 (1988).
43. Evans, J. W., Wainwright, M. S., Bridgewater, A. J., and Young, D. J., *Appl. Catal.* **7,** 75 (1983).
44. Denise, B., Sneeden, R. P. A., Beguin, B., and Cherifi, O., *Appl. Catal.* **30,** 353 (1987).
45. Tauster, S. J., *Acc. Chem. Res.* **20,** 389 (1987).
46. Haller, G. L., and Resasco, D. E., *Adv. Catal.* **36,** 173 (1989).
47. Delk, F. S., II, and Vavere, A., *J. Catal.* **85,** 380 (1984).
48. Del Arco, M., Caballero, A., Malet, P., and Rives, V., *J. Catal.* **113,** 120 (1988).
49. Cunningham, J., Al-Sayyed, G. H., Cronin, J. A., Healy, C., and Hirschwald, W., *Appl. Catal.* **25,** 129 (1986).
50. Cunningham, J., Al-Sayyed, G. H., Cronin, J. A., Fierro, J. L. G., Healy, C., Hirschwald, W., Ilyas, M., and Tobin, J. P., *J. Catal.* **102,** 160 (1986).
51. Cunningham, J., McNamara, D., Fierro, J. L. G., and O'Brien, S., *Appl. Catal.* **35,** 381 (1987).
52. Pepe, F., Polini, R., and Stoppa, L., *Catal. Lett.* **14,** 15 (1992).
53. Fleisch, T. H., and Mieville, R. L., *J. Catal.* **90,** 165 (1984).
54. Fleisch, T. H., and Mieville, R. L., *J. Catal.* **97,** 284 (1985).